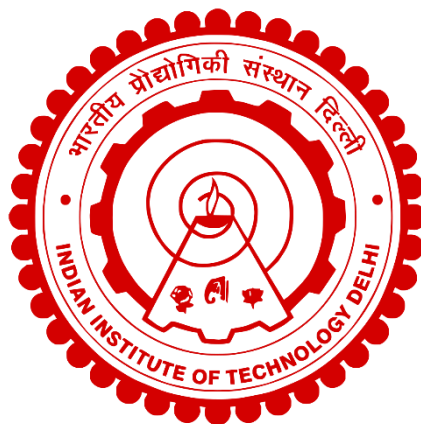


**EXPERIMENTAL AND NUMERICAL INVESTIGATIONS ON
MECHANICAL RESPONSE OF ALUMINUM AA2014-T6 UNDER
EXTREME LOADING & TEMPERATURE CONDITIONS**

ANOOP KUMAR PANDOURIA



**DEPARTMENT OF APPLIED MECHANICS
INDIAN INSTITUTE OF TECHNOLOGY DELHI**

JUNE 2023

© Indian Institute of Technology Delhi (IITD), New Delhi, 2023

**EXPERIMENTAL AND NUMERICAL INVESTIGATIONS ON
MECHANICAL RESPONSE OF ALUMINUM AA2014-T6 UNDER
EXTREME LOADING & TEMPERATURE CONDITIONS**

by

ANOOP KUMAR PANDOURIA

Department of Applied Mechanics

Submitted

in fulfilment of the requirements of the degree of Doctor of Philosophy

to the



INDIAN INSTITUTE OF TECHNOLOGY DELHI

JUNE 2023

Dedicated to my Parents and Teachers

CERTIFICATE

This is to certify that the thesis entitled “*Experimental and Numerical Investigations on Mechanical Response of Aluminum AA2014-T6 Under Extreme Loading & Temperature Conditions*” being submitted by **Mr. Anoop Kumar Pandouria** to the **Indian Institute of Technology Delhi**, for the award of the degree of **Doctor of Philosophy** in Applied Mechanics is a record of bonafide research work carried out by him under my supervision and guidance.

Mr. Anoop Kumar Pandouria has fulfilled all the prescribed requirements and the thesis is, in my opinion, worthy of consideration for the degree of Doctor of Philosophy in accordance with the regulations of the Institute. The contents of this thesis have not been submitted in part or in full to any other University or Institute for the award of any degree or diploma.

Dr. Vikrant Tiwari

Associate Professor

Department of Applied Mechanics

Indian Institute of Technology Delhi

New Delhi-110016

India

ACKNOWLEDGEMENTS

I would like to express my deepest gratitude to my supervisor, *Prof. Vikrant Tiwari*, for his patience, guidance, and support. I have tremendously benefited from his extensive expertise and careful editing. I am incredibly grateful that he accepted me as a student and kept his faith in me over the years. I will find opportunities to work with him in the future and learn from him. He has been helpful in developing my research attitude by highlighting my shortcomings and suggesting ways to improve them.

I would like to extend my sincere gratitude to the SRC committee members Prof. Rajesh Prasad, Prof. Maloy K. Singha, and Prof. Ashish K. Darpe for their continuous encouragement. Their insightful suggestions and feedback have assisted me in tackling and overcoming many problems during my research work.

I would like to thank my colleagues Dr. Danish Iqbal, Dr. Sanjay Kumar, Dr. Amit Kumar, Purnashis Chakraborty, Kuldeep Yadav, Rohit Kumar, Muddu Rahul Bharadwaj, and Palak Bhagoria for their encouragement during the most challenging phase of my Ph.D. I have also made some wonderful friends during my research work at IIT Delhi. I wish to thank Prashant, Vickey, Deepak, Navin, Mohit, Adnan, Babu, Anuj, Anurag, Bashir, Sriram, Hassan, Sajan Wahi, Mayank, and Krishan for their continuous support.

I would also like to acknowledge some close friends: Manoj Goyal, Upendra Bhaskar, Manoj Raipuria, Sushil Raipuria, Amit Pandouria, Sonu Gaur, Rajveer Garg, Durgesh Sonwar, and the late Deepak Kumar, who were always ready to help with any kind of

problem.

Also, thanks are due to Mr. Madan, Mr. Rishi, Mr. Anil, and Mr. Dinesh for their help in conducting experiments at the "workshop", "MTS", and "strength of materials" labs in the Applied Mechanics Department.

I am thankful for my parents, **Mr. Bhallu Ram Pandouria** and **Mrs. Malti Pandouria**, whose unwavering love and support keep me motivated and certain. My achievements and success are a result of their faith in me. I am also grateful for my uncle, **Mr. Ram Singh Jatav**, for his blessings and encouragements at every step. My deepest appreciation goes to my siblings, who keep me grounded, remind me of what is essential in life, and are always supportive of my endeavours. Lastly, I express my heartfelt gratitude to Ms. Preeti Chaurasiya, my wife. I will be forever thankful for the unconditional love and assistance I received during the entire thesis writing process and every day.

Anoop Kumar Pandouria

ABSTRACT

The present study focus towards understanding the mechanical response of AA2014-T6 alloy under static, dynamic, and impact loading conditions. Fracture behavior of any materials can be described by the characteristics like fracture initiation toughness and propagation toughness, which in turn depends on the strain rate and temperature. Research effort in this study can be summarized in the following steps. First, the material was characterized under tension and compression at different strain rates (10^{-4} to 10^3 s^{-1}) and temperatures (25 to 250 °C). Tensile and compression experiments at low strain rates (10^{-4} to 10^{-1} s^{-1}) were performed on conventional UTM equipped with the thermal heating chamber. High strain rate ($>10^3$ s^{-1}) experiments were carried out on SHPB (compression) and TSHPB (tension). Material was found to exhibit positive strain rate sensitivity and negative thermal rate softening for the considered strain rates and temperatures. Also, the strain hardening rate under compressive ultimate stress was observed to be higher when compared with the strain hardening rate under compressive yield stress. However, tensile yield and ultimate stress followed similar profile of strain hardening rate. Constitutive and fracture model parameters were evaluated to predict the plastic flow and fracture behavior of this alloy. In the considered constitutive model, plastic flow stress is the function of strain, strain rate, and temperature while the fracture strain is the function of stress triaxiality, strain rate and temperature. These parameters predicted flow stress with minimal error under both tension and compression loading.

Secondly, the fracture initiation and propagation toughness under static and dynamic loading were determined at a wide temperature range. Static fracture initiation

toughness was evaluated as per the ASTM E399 standard, while the modified Hopkinson pressure bar (MHPB) approach was used for dynamic fracture toughness. Identical pre-cracked three-point bend specimens were used for both static and dynamic experiments. A non-contact technique, 3D digital image correlation (DIC), was also used in this study to calculate the crack initiation time and crack mouth opening displacements, which were then used in determining the fracture characteristics. From experimental results, it was observed that the values of both dynamic fracture initiation and propagation toughness are higher as compared to static fracture initiation and propagation toughness. It was also found that the static fracture initiation toughness decreases continuously whereas propagation toughness increases with increase in temperature. Although, dynamic fracture initiation toughness attains the highest value at room temperature while the dynamic propagation toughness continuously increases with the increasing temperature. Further, a FE model was developed to incorporate the material constants and predict the fracture behavior of 3-point bend specimen under dynamic loading conditions. Numerical results of dynamic experiments found to be quite similar to the experiment results.

Lastly, the projectile impact experiments were performed on two different thickness monolithic plates (1 mm and 2 mm thick) and one homo-stacked configuration of 1_1 mm thick plate under blunt and hemispherical impacts. A single-stage gas gun coupled with ultra-high-speed synchronized cameras were used for this study. Captured images by the cameras were processed in Vic-3D software to get full-field deformation profile of the target plates. The experimental study reveals that the perforation of the plate is strongly influenced by the shape of the projectiles and plate thickness. Radial cracks were observed around the circumference of perforation hole when impacted by the

hemispherical projectile, while the shear failure was observed in case of the blunt projectile impact. A numerical simulation of projectile impact experiments was also performed using Johnson-Cook damage criteria to validate the experiment results. After comparison it was observed that both the experimental as well as simulations results are in good agreement with each other.

वर्तमान अध्ययन स्थिर, गतिशील और प्रभाव लोडिंग स्थितियों के तहत AA2014-T6 मिश्र धातु की यांत्रिक प्रतिक्रिया को समझने पर केंद्रित है। किसी भी सामग्री के फ्रैक्चर व्यवहार को फ्रैक्चर प्रारंभिक और प्रसार कठोरता जैसी विशेषताओं द्वारा वर्णित किया जा सकता है, जो तनाव दर और तापमान पर निर्भर करता है। इस अध्ययन में अनुसंधान प्रयास को निम्नलिखित चरणों में संक्षेपित किया जा सकता है। सबसे पहले, सामग्री को विभिन्न तनाव दरों (10^{-4} से 10^3 प्रति सेकंड) और तापमान (25 से 250 डिग्री सेल्सियस) पर तनाव और संपीड़न के तहत चित्रित किया गया है। थर्मल हीटिंग चैंबर से सुसज्जित पारंपरिक यूटीएम पर कम तनाव दर (10^{-4} से 10^{-1} प्रति सेकंड) पर तन्यता और संपीड़न प्रयोग किए गए। एसएचपीबी (संपीड़न) और टीएसएचपीबी (तनाव) पर उच्च तनाव दर ($>10^3$ प्रति सेकंड) प्रयोग किए गए। सामग्री को तनाव दर और तापमान के लिए सकारात्मक तनाव दर संवेदनशीलता और नकारात्मक थर्मल दर नरमी प्रदर्शित करने के लिए पाया गया। इसके अलावा, संपीड़ित उपज तनाव के तहत तनाव सख्त होने की दर की तुलना में संपीड़न परम तनाव के तहत तनाव सख्त होने की दर अधिक देखी गई। हालाँकि, तन्यता उपज और अंतिम तनाव ने तनाव सख्त होने की दर के समान प्रोफ़ाइल का अनुसरण किया। इस मिश्र धातु के प्लास्टिक प्रवाह और फ्रैक्चर व्यवहार की भविष्यवाणी करने के लिए संरचनात्मक और फ्रैक्चर मॉडल मापदंडों का मूल्यांकन किया गया है। विचारित संवैधानिक मॉडल में, प्लास्टिक प्रवाह तनाव - तनाव, तनाव दर और तापमान पर निर्भर करता है जबकि फ्रैक्चर तनाव - तनाव त्रिअक्षीयता, तनाव दर और तापमान पर निर्भर करता है। इन मापदंडों ने तनाव और संपीड़न लोडिंग दोनों के तहत न्यूनतम त्रुटि के साथ प्रवाह तनाव की भविष्यवाणी की।

इसके बाद, स्थैतिक और गतिशील लोडिंग के तहत फ्रैक्चर की प्रारंभिक और प्रसार कठोरता को एक विस्तृत तापमान सीमा पर निर्धारित किया गया है। स्थैतिक प्रारंभिक कठोरता का मूल्यांकन ASTM E399 मानक के अनुसार किया गया है, जबकि संशोधित स्प्लिट हॉपकिंसन प्रेशर बार (एमएचपीबी) सेटअप का उपयोग गतिशील फ्रैक्चर कठोरता के लिए किया गया है। स्थिर और गतिशील दोनों प्रयोगों के लिए समान पूर्व क्रैक थ्री-पॉइंट बेंड नमूनों का उपयोग किया गया है। इस अध्ययन में क्रैक आरंभ होने के समय और क्रैक माउथ ओपनिंग विस्थापन की गणना करने के लिए एक गैर-संपर्क तकनीक, 3-डी डिजिटल छवि सहसंबंध (डीआईसी) का भी उपयोग किया गया है, जिसके बाद इसका उपयोग फ्रैक्चर विशेषताओं को निर्धारित करने में किया गया है। प्रायोगिक परिणामों से, यह देखा गया कि गतिशील फ्रैक्चर प्रारंभिक और प्रसार कठोरता दोनों के मूल्य स्थैतिक फ्रैक्चर प्रारंभिक और प्रसार कठोरता की तुलना में अधिक हैं। यह भी पाया गया कि तापमान में वृद्धि के साथ स्थैतिक फ्रैक्चर प्रारंभिक कठोरता लगातार कम होती जाती है जबकि प्रसार कठोरता बढ़ती जाती है। हालाँकि, गतिशील फ्रैक्चर प्रारंभिक कठोरता कमरे के तापमान पर उच्चतम मूल्य प्राप्त करती है जबकि गतिशील प्रसार कठोरता बढ़ते तापमान के साथ लगातार बढ़ती है। इसके अलावा, सामग्री स्थिरांक को शामिल करने और गतिशील लोडिंग स्थितियों के तहत थ्री-पॉइंट बेंड नमूने के फ्रैक्चर व्यवहार की भविष्यवाणी करने के लिए एक 3-डी एफई मॉडल विकसित किया गया है। गतिशील फ्रैक्चर घटनाओं के सिमुलेशन परिणाम प्रयोग परिणामों के काफी समान पाए गए।

अंत में, प्रक्षेप्य प्रभाव प्रयोग दो अलग-अलग मोटाई की मोनोलिथिक प्लेटों (1 मिमी और 2 मिमी मोटी) और 1_1 मिमी मोटी प्लेट के एक होमो-स्टैकड कॉन्फ़िगरेशन पर ब्लंट और हेमीस्फेरिकल प्रभावों के तहत किए गए हैं। इस अध्ययन के लिए अल्ट्रा-हाई-स्पीड सिंक्रोनाइज़्ड कैमरों के साथ सिंगल स्टेज गैस गन का उपयोग किया गया है। लक्ष्य प्लेटों की पूर्ण-क्षेत्र विरूपण प्रोफ़ाइल

प्राप्त करने के लिए कैमरों द्वारा कैप्चर की गई छवियों को विक-3डी सॉफ्टवेयर में संसाधित किया गया। प्रायोगिक अध्ययन से पता चलता है कि प्लेट का छिद्र प्रक्षेप्य के आकार और प्लेट की मोटाई से काफी प्रभावित होता है। हेमीस्फेरिकल प्रक्षेप्य से प्रभावित होने पर वेध छेद की परिधि के आसपास रेडियल दरारें देखी गईं, जबकि ब्लंट प्रक्षेप्य प्रभाव के मामले में कतरनी विफलता देखी गई। प्रयोग के परिणामों को मान्य करने के लिए जॉनसन-कुक क्षति मानदंड का उपयोग करके प्रक्षेप्य प्रभाव प्रयोगों का एक संख्यात्मक अनुकरण भी किया गया है। तुलना के बाद यह देखा गया कि प्रयोगात्मक और सिमुलेशन दोनों परिणाम एक-दूसरे के साथ अच्छे अनुरूप हैं।

Table of Contents

CERTIFICATE	VII
ACKNOWLEDGEMENTS	IX
ABSTRACT	XI
TABLE OF CONTENTS	XVII
LIST OF FIGURES	XXIII
LIST OF TABLES	XXIX
INTRODUCTION AND OBJECTIVES	1
1.1 INTRODUCTION.....	1
1.2 BRIEF REVIEW ON EXPERIMENTAL SETUPS AND MEASUREMENTS TECHNIQUES ...	3
1.3 LITERATURE GAP	4
1.4 OBJECTIVES.....	7
1.5 SOLUTION APPROACH FOR THE CURRENT STUDY	8
1.6 STRUCTURE OF THESIS	8
COMPRESSIVE AND TENSILE BEHAVIOR OF AA2014-T6 UNDER DIFFERENT STRAIN RATES AND DIFFERENT TEMPERATURES	11
2.1 INTRODUCTION.....	12
2.2 EXPERIMENTAL PROCEDURE	18
2.2.1 Specimen material	18
2.2.2 Quasi-static uniaxial compression and tensile experiments	19
2.2.3 Dynamic compression and tensile experiments.....	20
2.3 RESULTS AND DISCUSSION	22
2.3.1 Tensile and compressive behavior of AA2014-T6.....	22
2.3.2 Strain rate effect.....	29

2.3.3 Temperature effect.....	31
2.3.4 Strength differential effect.....	33
2.4 CONSTITUTIVE MODEL.....	34
2.4.1 Determination of material parameter A, B, and n	35
2.4.2 Determination of material parameter C	36
2.4.3 Determination of material parameter m.....	37
2.4.4 Error estimation	39
2.5 CONCLUSIONS	40

**INVESTIGATIONS INTO THE STATIC AND DYNAMIC FRACTURE
INITIATION AND PROPAGATION TOUGHNESS OF AA2014-T6
INCORPORATING TEMPERATURES EFFECTS..... 43**

3.1 INTRODUCTION.....	44
3.2 FORMULATIONS.....	49
3.2.1 Static fracture initiation toughness	49
3.2.2 Dynamic fracture initiation toughness.....	51
3.2.3 Procedure for propagation toughness measurement.....	52
3.3 EXPERIMENTAL SETUP AND MEASURING TECHNIQUES	53
3.3.1 Experimental setup	53
3.3.2 Temperature measurements	55
3.3.3 Material and specimen.....	56
3.3.4 Fatigue crack.....	57
3.4 EXPERIMENTAL RESULTS AND DISCUSSION	58
3.4.1 Static fracture initiation and propagation toughness	58
3.4.2 Dynamic fracture initiation and propagation toughness.....	63
3.5 CONCLUSIONS	72

MATERIAL DAMAGE MODELLING AND NUMERICAL SIMULATION OF ALUMINUM AA2014-T6 SPECIMENS UNDER DYNAMIC TENSILE AND 3-POINT BEND LOADING	75
4.1 INTRODUCTION.....	76
4.2 MATERIAL, SPECIMENS, AND EXPERIMENTS.....	79
4.3 FINITE ELEMENT MODEL.....	81
4.3.1 Dynamic 3-point bend experiment	81
4.3.2 High strain rate tensile experiment.....	82
4.4 EXPERIMENTAL RESULTS AND DISCUSSION	83
4.4.1 Effect of temperature and strain rate	83
4.4.2 Effect of stress triaxiality.....	84
4.4.3 Material constitutive model	85
4.4.4 Material failure model	86
4.4.5 Dynamic fracture toughness experiments.....	87
4.5 NUMERICAL RESULTS AND COMPARISON WITH EXPERIMENTAL RESULTS	92
4.5.1 Numerical results of dynamic 3-point bend experiments.....	92
4.5.2 Numerical results for high strain rate tensile experiments	95
4.6 CONCLUSIONS	97
EVALUATION OF AA2014-T6 PLATE RESPONSE WHEN SUBJECTED TO THE PROJECTILE IMPACT	99
5.1 INTRODUCTION.....	100
5.2 EXPERIMENTAL PROCEDURE	104
5.2.1 Experimental and imaging setup	104
5.2.2 Target plate configuration and projectiles	106
5.3 NUMERICAL MODELLING OF PROJECTILE IMPACT.....	108
5.4 RESULTS AND DISCUSSION	110

5.4.1 Effect of projectile nose shape.....	110
5.4.2 Effect of target plate thickness and homo-stacking.....	113
5.4.3 Post impact analysis of target plates and ejected plug.....	115
5.4.4 Comparison of numerical and experimental results	117
5.5 CONCLUSIONS	120
CONCLUSIONS AND FUTURE WORK.....	123
6.1 SUMMARY AND CONCLUSIONS	123
6.2 FUTURE WORK	125
REFERENCES.....	127
LIST OF PUBLICATIONS	143
AUTHOR’S BIODATA.....	145

List of Figures

Figure 2.1 Actual pictures of the specimen used in (a) quasi-static compression, (b) quasi-static tension, (c) dynamic compression, and (d) dynamic tension experiments.....	20
Figure 2.2 The schematic diagram of (a) tensile SHPB (b) compression SHPB.....	21
Figure 2.3 Typical experimental data obtained from SHPB compression experiments representing (a) strain-time history (b) time shifted strain signal and corresponding (c) force equilibrium (d) stress-strain curve.....	24
Figure 2.4 Plastic flow stress under compressive loading at different strain rate for temperature (a) 25 °C (b) 100 °C (c) 150 °C (d) 200 °C (e) 250 °C.....	25
Figure 2.5 Deformed specimens under compressive loading (static and dynamic) at different temperatures.....	26
Figure 2.6 Plastic flow stress under tensile loading at different strain rate for temperature (a) 25 °C (b) 100 °C (c) 150 °C (d) 200 °C (e) 250 °C.....	27
Figure 2.7 Fractured surface of tensile specimens at different temperatures used in this study.....	28
Figure 2.8 Variation of (a) yield stress and (b) ultimate stress with different strain rates at 25 °C and 250 °C.....	30
Figure 2.9 Plastic flow stress under compressive loading at different temperature for strain rate (a) 10^{-4} s^{-1} (b) 10^3 s^{-1}	31
Figure 2.10 Plastic flow stress under tensile loading at different temperature for strain rate (a) 10^{-4} s^{-1} (b) 10^3 s^{-1}	32

Figure 2.11 Variation of (a) yield stress and (b) ultimate stress with temperature at 10^4 s^{-1} and 10^3 s^{-1}	33
Figure 2.12 Linear curve fitting of $\ln(\sigma - A) - \ln(\dot{\epsilon})$ for (a) tension and (b) compression.....	36
Figure 2.13 Linear curve fitting of $\{(\sigma_{HS} / \sigma_{RS}) - 1\}$ and $\ln(10^4 \dot{\epsilon})$ for (a) tension and (b) compression.....	37
Figure 2.14 Linear curve fitting of $\ln[1 - (\sigma_{HT} / \sigma_{RT})]$ and $\ln(T^*)$ for (a) tension and (b) compression.....	38
Figure 2.15 Comparison of JC model with experimental results under (a) tension and (b) compression.....	39
Figure 3.1 Geometry and ROI of 3-point bend test specimen.....	50
Figure 3.2 Process of measuring load P_Q using Load vs CMOD plot.....	51
Figure 3.3 Schematic diagram of MHPB setup used in this study.....	54
Figure 3.4 True stress vs true strain curve of AA2014-T6.....	57
Figure 3.5 Specimen subjected to cyclic loading to induce pre-crack before the experiments.....	57
Figure 3.6 Experimental setup for static 3-point bend experiments at different temperatures.....	59
Figure 3.7 Typical Comparison between DIC and clip gauge measurement of CMOD.....	60
Figure 3.8 Total absorbed energy and Load vs CMOD to determine the propagation toughness in static condition.....	60
Figure 3.9 Load-CMOD curves at different displacement rate of static 3-point test.....	60

Figure 3.10 Load vs CMOD profile with various temperature range at test speed of (a) 1 mm/min and (b) 100 mm/min.....	62
Figure 3.11 Temperature effect on static fracture initiation and propagation toughness at displacement rate of (a) 1 mm/min and (b) 100 mm/min.....	63
Figure 3.12 Experimental set-up for dynamic 3-point bend experiments along with thermal facility.....	64
Figure 3.13 Voltage-time history recorded by strain gauge mounted on Hopkinson bar.....	65
Figure 3.14 Comparison of LPD-time history measurement with DIC and strain gauge signals.....	66
Figure 3.15 Undeformed and deformed speckle surfaces along with their comparison plots of LPD at (a) -150 °C, (b) RT, and (c) 200 °C.....	67
Figure 3.16 Von Mises strain profile at different time intervals for a 3-point bend specimen under the projectile impact velocity of 13.46 m/s.....	68
Figure 3.17 Dynamic force and LPD (u) curve at different temperature of dynamic 3-point bend test.....	69
Figure 3.18 Dynamic SIF- time response at different temperature.....	70
Figure 3.19 Dynamic force and total absorbed energy variation with load point displacement at room temperature and 100 °C.....	71
Figure 3.20 Dynamic fracture initiation and propagation toughness under different temperatures.....	71
Figure 4.1 Pictures of actual test specimens used for (a) stress triaxiality, (b) static tensile, (c) high strain rate tensile, and (d) three-point bend experiments.....	81
Figure 4.2 Meshed model used for simulating the (a) dynamic 3-point bend experiment and (b) tensile experiments at high strain rate.....	83

Figure 4.3 True stress and true strain curve at different (a) temperatures and (b) strain rates.....	84
Figure 4.4 True stress and true strain curve at different stress triaxiality.....	85
Figure 4.5 The plastic flow stress of AA2014-T6 alloy as a function of (a) strain hardening, (b) strain rate hardening, and (c) temperature.....	86
Figure 4.6 The fracture strain of AA2014-T6 alloy as a function of (a) stress triaxiality, (b) strain rate, and (c) temperature.....	87
Figure 4.7 Effect of projectile velocity on DSIF (K_I) with respect to time.....	88
Figure 4.8 Von Mises strain field around the crack tip at the time of crack initiation for dynamic 3-point bend experiments with different projectile velocities.....	90
Figure 4.9 Applied Load and total energy absorbed by the specimen up to the fracture at different projectile velocities of (a) 10.13 m/s, (b) 13.68 m/s, (c) 15.97 m/s, (d) 17.37 m/s, and (e) 19.59 m/s.....	91
Figure 4.10 Effect of loading rate on the DFIT (K_{I_d}) and DFPT ($K_{I_d}^P$).....	91
Figure 4.11 Incident stress obtained from dynamic experiment at impact velocity of 15.97 m/s.....	92
Figure 4.12 Stress distribution of simulated TPB specimen at different time intervals under the impact velocity of 15.97 m/s.....	93
Figure 4.13 Comparison of numerical results with the (a) CMOD measured using 3D DIC and (b) LPD obtained from strain gauge, during dynamic 3-point bend experiments at projectile velocity of 15.97 m/s.....	95
Figure 4.14 Comparison of experimental and numerical contours for displacement (v) perpendicular to the crack plane at different time intervals under the impact velocity of 15.97 m/s.....	96

Figure 4.15 Comparison of the tensile SHPB experiment and simulation results by comparing (a) plastic flow stress and strain, and full field contour of local strain distribution obtained (b) numerically and (c) experimentally.....	97
Figure 5.1 (a) Schematic representation of experimental setup (b) Actual experimental setup with ultra-high speed imaging system.....	105
Figure 5.2 Actual photographs of (a) target plate, (b) blunt projectile, and (c) hemispherical projectile along with their dimensions.....	107
Figure 5.3 Meshed model of target plate used in this study.....	110
Figure 5.4 Full field out-of-plane displacement profile at different time intervals for 2 mm thick plate impacted by (a) blunt and (b) hemispherical projectile at impact velocity of 152 m/s and 156 m/s, respectively.....	111
Figure 5.5 Transient out-of-plane displacement (a-c), velocity (d-f), and acceleration (g-e) of 2 mm thick plate impacted by blunt and hemispherical projectile at an impact velocity of 152 m/s and 156 m/s, respectively.....	112
Figure 5.6 Out-of-plane displacement of target plates impacted by blunt projectile (a-c) and hemispherical projectile (d-f) at impact velocity of 218 m/s and 225 m/s, respectively.....	114
Figure 5.7 Maximum out-of-displacement for different configuration of target plates impacted by (a) blunt and (b) hemispherical projectile.....	115
Figure 5.8 Perforated plates and ejected plugs for different configurations impacted by blunt (218 m/s) and hemispherical (225 m/s) projectile at different impact velocities.....	116
Figure 5.9 Numerically obtained out-of-plane deformation for all the target plate configuration impacted by hemispherical and blunt projectile at a selected impact velocity of 155 m/s.....	117

Figure 5.10 Comparison of deformation (W) near the impact zone (point P) obtained numerically and experimentally for the different configuration of target plates impacted by blunt projectile (a-c) and hemispherical projectile (d-f) at an impact velocity of 155 m/s.....119

Figure 5.11 Comparison of simulation results with the experimental results in term of failure mode, ejected plug size and hole diameter of target plate (2 mm thick) formed due to impact by (a) blunt and (b) hemispherical projectiles at an impact velocity of 155 m/s.....120

List of Tables

Table 1.1. J-C models parameters for different aluminum alloys.....	5
Table 1.2. Static and dynamic fracture toughness for various ductile materials.....	6
Table 2.1. Chemical composition (in wt.%) of AA2014-T6 alloy.....	19
Table 2.2. Tensile experimental results at room temperature (25 °C) under different strain rates.....	29
Table 2.3. Compression experimental results at room temperature (25 °C) under different strain rates.....	29
Table 2.4. Tensile experimental results at reference strain rate (10^{-4} s^{-1}) with various temperatures.....	32
Table 2.5. Compression experimental results at reference strain rate (10^{-4} s^{-1}) with various temperatures.....	33
Table 2.6. Strength differential effect of yield strength.....	34
Table 2.7. Johnson-Cook constitutive model parameter of AA2014-T6.....	38
Table 2.8. The absolute average error ($\Delta_{avg.}$) and correlation coefficient (R) values.....	40
Table 3.1. Mechanical properties of AA2014-T6 alloy.....	56
Table 3.2. Experimental results of static 3-point bend test.....	61
Table 3.3. Experimental results of dynamic 3-point bend test.....	72
Table 4.1. J-C parameters for Aluminum AA2014-T6 obtained in this study.....	87
Table 4.2. Summary of dynamic 3-point bend experiments at different loading rates.....	89

Table 5.1. Important parameters related to 3D-DIC experimental setup..... 106

Table 5.2. Details of experiments target plate configuration and impact velocity... 108

Table 5.3. Russell error values at an impact velocity of 155 m/s corresponding to the
point ‘P’..... 118